COBEM 2023 27TH INTERNATIONAL CONGRESS OF MECHANICAL ENGENEERING

ABCM Brazilian Society of Mechanical Sciences and Engineering
27th ABCM International Congress of Mechanical Engineering
December 04-08, 2023, Florianópolis-SC, Brazil

COB-2023-1668
AERODYNAMIC ANALYSIS OF A FSAE VEHICLE OF THE UFVOLTS MAJORADOS TEAM THROUGH CHANGES IN END PLATES DESIGN

Ainara Mendes de Paula
Joseph Kalil Khoury Junior
Geice Paula Villibor
Universidade Federal de Viçosa – UFV, Av. Peter Henry Rolfs, s/n, Campus Universitário, Viçosa, MG, Brazil
ainara.paula@ufv.br, kalil@ufv.br, geice.villibor@ufv.br

Abstract. *Aerodynamic vehicle analysis is an important tool to determine parameters of the airflow over it. The aerodynamic design of racing cars aims, mainly, at producing down force and keeping the drag force at low levels. In Formula SAE (FSAE) racing vehicles, the wings are primarily responsible for bringing the center of negative lift closer to the axles, changing the normal force of the tire against the ground, increasing friction, and making the vehicle more stable in corners. Therefore, the objective is to analyze the aerodynamic design of the UFVolts Majorados FSAE team with the aid of computational fluid dynamics (CFD). The applied methodology complies with the FSAE Rules 2022, respecting the geometric constraints of the vehicle. The CAD designs were modeled in SolidWorks and the CFD simulations performed in ANSYS Fluent. A mesh independence study was carried out to verify that the results found by the program are independent of the mesh size used. After each simulation step, the aerodynamic coefficients were compared, as well as the aerodynamic efficiency of each studied model. Thus, the best configuration in terms of the lowest drag force coefficient for highest gain in down force was selected. The final assembly achieved a drag coefficient (C_D) of 0.898, a lift coefficient (C_L) of -1.2019 and an aerodynamic efficiency of 1.3375, representing 0.68% reduction in C_D, 20.0% increase in C_L, and improvement of 20.82% in efficiency compared to the initial design with front and rear wings.*

Keywords: *Race Car Aerodynamics, CFD simulation, FSAE, Design machine*

1. INTRODUCTION

The interaction of aerodynamics between air and a solid body in motion allows the calculation of the forces and moments acting on the object. However, the two goals of aerodynamics in the vehicles are down force and drag force, created by pressure gradients accordingly shear stress distribution on the surface of the body (MAIA, 2015).

Recently, the automobile industry has been investing more and more in improving the aerodynamic properties of its vehicles. The improvements include modifications to the fairing geometry and the incorporation of devices such as front wings, rear wings, and diffuser floors.

An option to produce more efficient racing cars is by understanding how the air flows around the body and its aerodynamic devices. A vehicle aerodynamically well designed can utilize airflow to produce down force and maintain drag force at lower levels (BARBOSA, 2018). In this way, increase the tire adherence and the car can reach higher speeds in the corners, reducing the lap time of the course, while there is a lower consumption of energy due to the reduced air resistance, even with at low average speed on Formula SAE competition circuits.

The objective was to analyze aerodynamic package parameter of the Formula SAE UFVolts Majorados team with the aid of computational fluid dynamics and through the modeling of new end plate geometries, prioritizing down force gain and drag reduction. In this way, the drag coefficients (C_D) and lift coefficients (C_L) parameters of the front and rear wings of the prototype could be compared. As well as the aerodynamic efficiency of each model was studied, providing a database that helped in the understanding and better use of it. Therefore, it was possible to define the best set and the influence of the new aerodynamic package.

2. MATERIAL AND METHODOS

The CAD car designs were modeled in SolidWorks and the CFD simulations performed in ANSYS Fluent. Intel Core i7-7200U processor, with 3.5 GHz and 16 GB of RAM memory computer were used to run program.

2.1. Modeling Conditions

1.1.1 Control volume model

The modeling represents the main characteristics or features that affect the flow. The control volume for the simulations was generated following the recommendations shown in Figure 1 considering the upper extremes of the dimensions, being five lengths of the vehicle in front and eight lengths behind, a height six times greater than the height of the vehicle and the width ten times its width (CD-ADAPCO, 2015 apud SOLIMAN, 2015). Furthermore, due to the high symmetry of the prototype, only half a domain was used in the analyses.

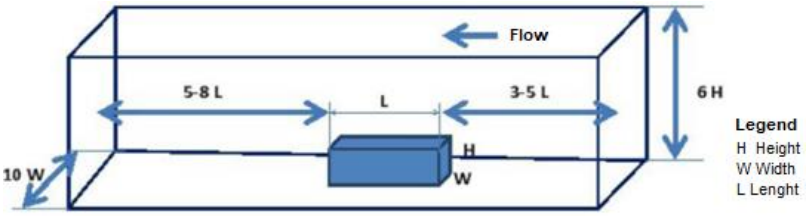

Figure 1. Control volume dimensions used for ground vehicle aerodynamics (Adapted of the CD-ADAPCO, 2015 apud SOLIMAN, 2015).

2.1.1. Mesh generation

Pressure distribution is strongly affected by flow separation and replacement locations. Therefore, it is important that the surface mesh solves all relevant geometry details and figure out the requirements of the physical models used in the simulation (LANFRIT, 2005). Therefore, to ensure low asymmetry elements where viscous effects are large, prism elements were extruded from the surface of the object under study and the rest of the domain filled with tetrahedral elements.

Furthermore, to ensure a continuous growth of the tetrahedral elements up to the limits of the influence body, the element size was limited in the refinement controls. Following the recommendation of Lanfrit (2005), this value should be up to 200 mm. Table 1 shows a summary of the configurations used for mesh generation.

Table 1. General settings used for mesh generation.

Parameter	**Configuration**
Size function	Proximity and curvature
Smoothness	High
Method	Tetrahedrons
Algorithm	Patch independent
Inflation option	First layer thickness

2.1.2. Mesh quality

The important quality criterion for the fluid dynamic analysis is about the element quality for discretization. According to the definition of skewness, a value of zero indicates an equilateral cell and a value of one indicates a completely distorted cell. The skewness elements determine how a face or cell is close of the ideal (ANSYS, 2020). Highly inclined elements should be avoided because decrease accuracy and destabilize the solution. An ANSYS recommendation is that the maximum skewness should be below 0.98.

2.1.3. Independence mesh of the CFD

This study is based on increasing refinement of the mesh and running the simulations determining results of interest, which in this case will be the C_L and C_D. Naturally, as the level of refinement increases, the results will tend to converge for a value. Figure 2 shows the behavior of the C_L of the rear wings as a function of mesh refinement, about four levels. The C_L starts to have a little significant variation. For this reason, four levels were selected for performing the rear wing simulations. A similar procedure was followed to determine the mesh refinement level for the front wing and prototype assembly.

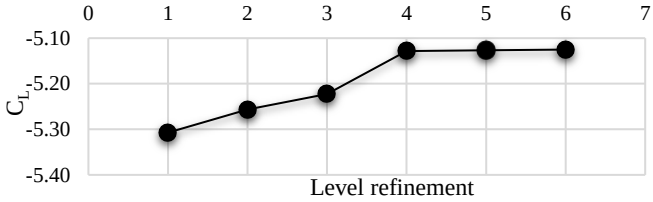

Figure 2. Lift coefficient (C_L) behavior as a function of mesh refinement for rear wing analyses.

2.1.4. Boundary conditions and solution configuration

The boundary conditions used to represent the models were:

- Input velocity of 16.67 m/s, with turbulence intensity of 1% and turbulent viscosity ratio equal to 10;
- Output pressure of 0 Pa, turbulent intensity of 5% and turbulent viscosity ratio equal to 10;
- Relative ground speed of 16.67 m/s, without slipping and translation in the same direction as the input speed.
- Angular wheel speed of 58.49 rad/s and no slip.

The turbulence model used was the k-ω SST belonging to the RANS methodology, which rigorously explains the anisotropy of turbulence and the transport of all Reynolds stresses (LANFRIT, 2005). This model is recommended for high-fidelity simulations.

The calculation was processed by the coupled scheme using equations of first order upwind in the first 50 iterations and of second order upwind in the remaining iterations.

2.2. Rear wing analysis

2.2.1. Rear wing

The aerodynamic profile chosen to compose the rear wing was the CH10, selected in the Airfoil Tools catalogue. According to McBeath (2017), for a two-element wing, the flap chord should be 25 – 30% of the main profile chord, the gap between the profiles 1 – 2% C and the flap overlap from 3 – 5% C.

Given that the chord of the main profile of the rear wing is equal to 400 mm and adopting the upper extremes of the intervals recommended by McBeath (2017), the flap chord 30% C (120 mm), the gap 2% C (8 mm) and the overlap 5%C (20 mm). Furthermore, analyzes carried out by the team indicated that the most effective angles of attack for the main profile and the flap are 5° and 35°, respectively. Figure 3 shows the dimensions and positioning of the profiles.

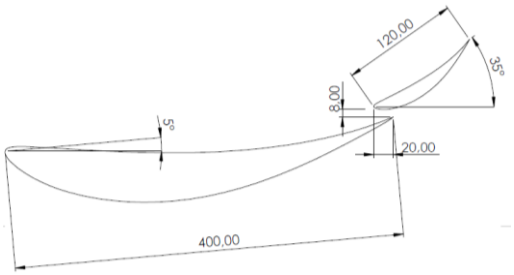

Figure 3. Rear wing configuration. Main profile: 400 mm of chord and 5° angle of attack; flap: 120 mm of chord and 35° angle of attack; gap: 8 mm and overlap: 20 mm.

The end plate models were numbered from 1 to 7, with end plates. The end plate from Table 2(1) was used in the GX-E03 prototype, followed by the other models obtained from the modification of this initial geometry and the other designs.

Table 2. End plates profile lateral view from rear wings.

1	2	3	4	5	6	7
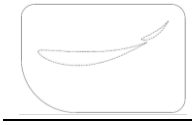	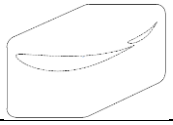	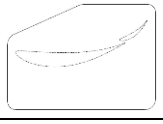	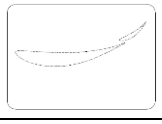	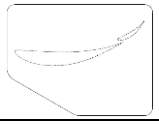	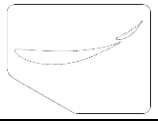	

2.2.2. End plates

The analysis started with the end plates used in the GX-E03 prototype (Table 2-1). Then, modifications were made to this geometry to obtain new models. The thickness of each end plate kept at 10 mm and the span at 980 mm. To obtain greater contact with the free flow, the rear wing must be in the highest position allowed by the competition regulations, 1.2 m from the ground.

Modifications were made to control or eliminate unwanted flows. Also, some of the CADs were modeled in a freeway, not following the pattern of the initial part and the CAD drawings were imported from the SolidWorks of the *parasolid (.x_t)* format.

2.3. Front wing analysis

2.3.1. Wing configuration

The same aerodynamic profile from CH10 prototype was selected to compose the front wing. As the main profile chord is equal to 300 mm, the flap chord corresponds to 20%C (60 mm), the gap 2%C (7 mm) and the overlap 3%C (10 mm). Furthermore, analyzes carried out by the team indicated that the most effective angles of attack for the main profile and front flap are 10° and 30°, respectively. Figure 4 shows the dimensions and positioning of the profiles.

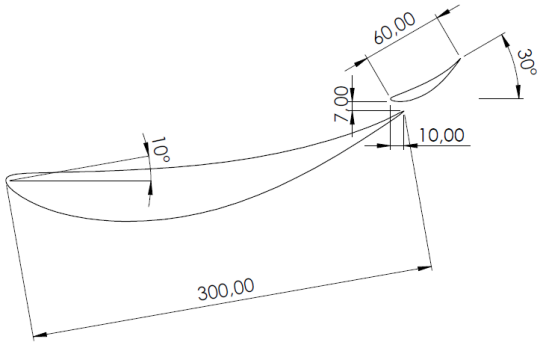

Figure 4. Front wing configuration: Main profile: 300 mm of chord and 10° angle of attack; flap: 60 mm of chord and 30° angle of attack; gap: 7 mm and overlap: 10 mm.

For the front wing the models were numbered from 1 to 3, with the end plate 1 being the component used in the GX-E03 prototype, followed by two modifications in this geometry. Due to the proximity of the wing to the ground and the dimensional limitations imposed by the competition regulations, there are few options left for the variation of this component. Table 3 presents a three-dimensional view of the wing mounted with the end plates tested.

Table 3. End plate's lateral view profiles from front wings.

1	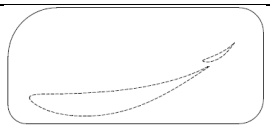	2	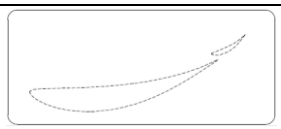	3	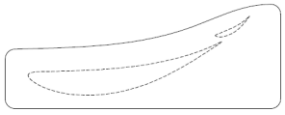

2.3.2. End plates

In the front wing, in addition to modifications in the geometries of the end plates, foot plates mounted perpendicularly to the end plates were implemented to reduce the flow that escapes under the end plate (SOLIMAN, 2015), as illustrated in Figure 5. The thickness of each end plate was also fixed at 10 mm and the wingspan at 1200 mm.

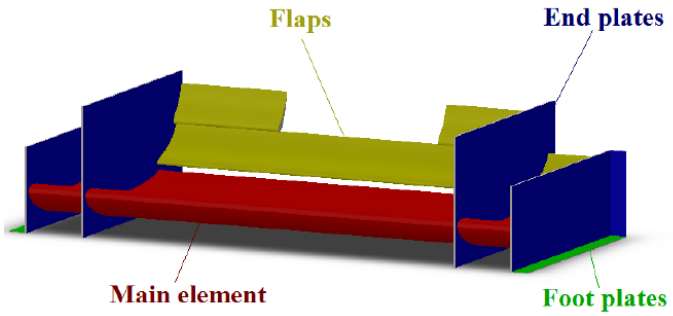

Figure 5. Components of a front wing, in red the main profile, in blue the end plates, in gold the flaps and in green the foot plates (SOLIMAN, 2015, p. 27.).

2.4. Model analysis

The initial simulation of the prototype was made with a model that considers only the volume occupied by the nose (nose cone), fairing, tires, a representation of the pilot and other external elements (Figure 6). Subsequently, this same model was used, with the addition of the front and rear wings, in their position of attachment to the structure.

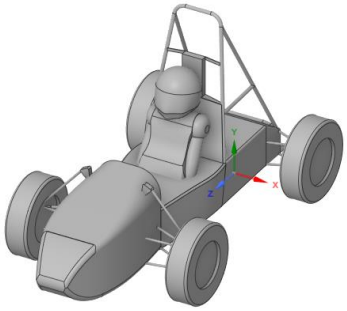

Figure 6. Simplified model with nose cone, fairing, tires, pilot, and other external elements.

The data obtained from the analysis of each modification in the components were organized in tables after each simulation step and aerodynamic coefficients compared. The aerodynamic efficiency of each model, defined by the ratio between the C_L and C_D. Thus, the set that proved to be the most viable was selected, respecting the maximum C_D of 1.20 defined by the team. Then a new assembly was made on the prototype, considering the chosen wing models. Finally, it was possible to analyze the loads generated and the influence of the new aerodynamic package. The judgment on the efficiency of the assemblies was limited to the comparison between the aerodynamic coefficients of the models obtained through the CFD simulations and the C_L/C_D ratios, this being the main characteristic that describes the overall aerodynamic performance.

3. RESULTS AND DISCUSSION

3.1. Initial design

Initial design without the wings were analyzed, the data summarized in Table 4 were obtained. The objective of this simulation is to determine the efficiency of the car without aerodynamic devices and to obtain its characteristics such as the frontal area and the C_D and C_L, to estimate amount aerodynamic devices will be able to improve this scenario.

Table 4. Data Simulation of the initial design car without wings.

Frontal area	0,8129 m²
C_D	0,8247
C_L	0,4287
C_L / C_D	0,5198

Without aerodynamic package the C_L is positive. Figure 7 shows the map of pressures and streamlines in the post-processing of the first analysis performed, where it is possible to observe zones of flow recirculation mainly in the space behind the pilot. At the simulated speed of 60 km/h, this model generates a total lift force of 29.66 N and a drag force of 57.06 N.

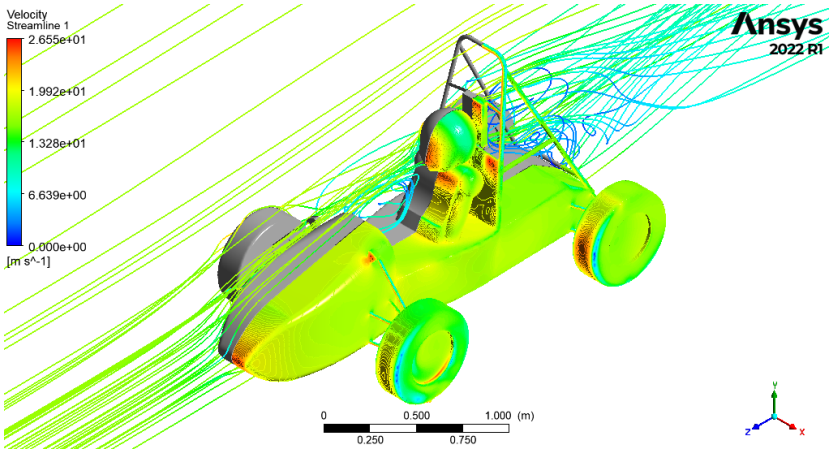

Figure 7. Pressure distributions and flow lines from car without wing.

To improve part of this problem, the front and rear wings were designed. The data obtained from the analysis after its assembly in the car are presented in Table 5.

Table 5. Aerodynamic data of the car with wings.

Frontal Area	1,0005 m²
C_D	0,9046
C_L	-1,0016
- C_L / C_D	1,1072

Figure 8 shows the pressure and streamline map of the car simulation after adding the wings. At the simulated speed of 60 km/h, this model generates a drag force of 98.56 N, almost twice as high as the previous model, while the down force has increased significantly to 236.29 N, which is about eight times larger than the model without the wings.

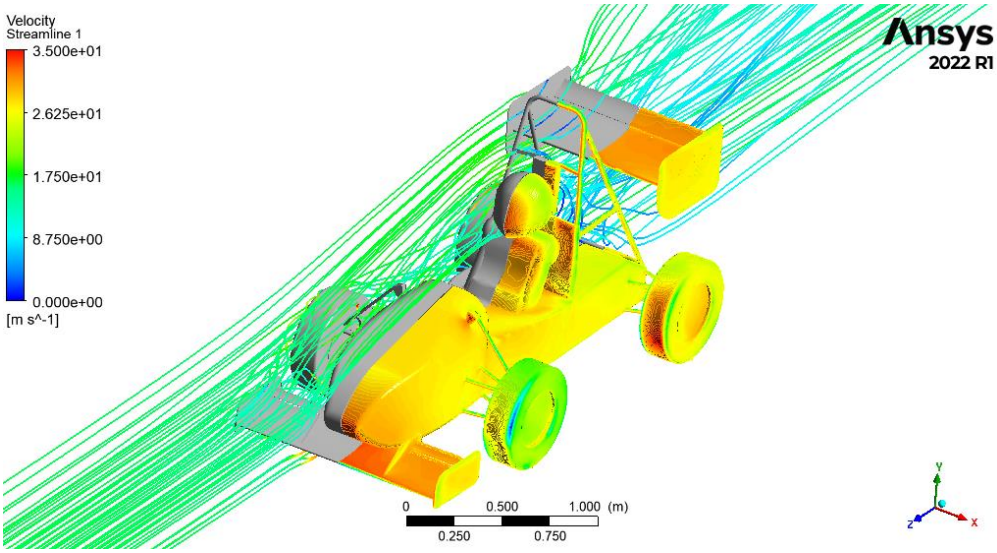

Figure 8. Pressure distributions and flow lines from car with wing.

3.2. Rear wings

Data simulations were summarized in Table 6, then the aerodynamic coefficients could be compared, as well as the efficiency aerodynamic of each model. The highlights represent the smallest $\mathbf{C}_D$, the highest $\mathbf{C}_L$ and the highest Efficiency Aerodynamic value.

Table 6. Summary of the aerodynamic characteristics of the end plate models tested for the rear wing, especially the smaller C_D, bigger C_L, and best aerodynamic efficiency from the $\mathbf{C_L/C_D}$ ratio.

End plate model	C_D	C_L	$-C_L/C_D$
1	1,0781	-5,4131	5,0210
2	**1,0096**	-5,0204	4,9727
3	1,0149	-5,1210	5,0458
4	1,0176	-5,1364	**5,0476**
5	1,0828	-5,3600	4,9501
6	1,1038	**-5,4571**	4,9439
7	1,0411	-5,1431	4,9401

Since the reference area of the wing had little variation independent of the model analyzed, the C_D is also close, with the largest variation of the order of 0.094.

Table 5 shows the wing with the end plate 2 has the lowest C_D. However, it also has the lowest C_D. The opposite happens with model 6, which has not only the highest C_L, but also the highest C_D, making it good for usage.

In addition, models 5, 6 and 7 have the worst results considering aerodynamic efficiency. One possible explanation for these lower values is that the increase in static pressure above the wing is smaller than the decrease in static pressure below it (MCBEATH, 2017). Thus, the influence wing is largest below than above it and, this means that is necessary the end plate to be larger below the wing.

Based on the $-C_L/C_D$ ratio, the best results are from models 1, 3 and 4, which cover a larger area below the profiles, especially in the lower rear region. Figure 9 shows the pressure map in the center of the wingspan with end plates 7 and 4, which have the lowest and highest $-C_L/C_D$ values, respectively. It is observed between Figure 9 a and b, that the wing with the end plate 4 has a region of lowest pressure, evidencing its higher aerodynamic efficiency about $\mathbf{C_L/C_D}$.

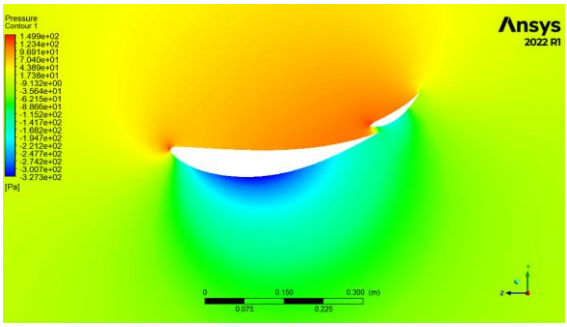

Figure 9.a) Pressure map at the center of the wingspan with end plate 7.

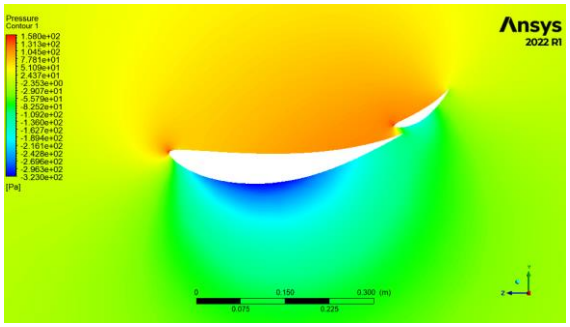

b) Pressure map at the center of the wingspan without end plate 4.

In the several variations tested, the end plate 3 model was selected to integrate the new rear wing because it has the second highest value of $\mathbf{C_L/C_D}$ and, mainly, one of the lowest C_D. In addition, cutting above the profiles on end plate 3 can benefit the assembly by reducing the weight of the element.

3.3. Front Wings

Similarly, to the rear wing, the data from the front wing simulations were summarized in Table 7, facilitating the comparison between the aerodynamic coefficient ratio and the aerodynamic efficiency of each model.

Table 7. Aerodynamic characteristics of the end plate models tested for the front wing, highlighting the smaller C_D, higher C_L and coefficients efficiency.

End Plates profile	C_D	C_L	$-C_L/C_D$
1	**0,7609**	-4,8950	6,4332
2	0,7646	-4,9701	**6,5003**
3	0,8644	**-5,4653**	6,3227

As highlighted in Table 7, the team-designed Profile 1 has the smallest C_D, but also the lowest C_L. Profile 3 obtained the highest C_L, accompanied by the highest C_D and the lowest efficiency ratio. Profile 2 has median values of coefficients, but with the highest aerodynamic efficiency.

For this reason, Profile 2 was selected to compose the new aerodynamic package and served as the basis for the analyses of proximity to the ground and addition of foot plates.

3.3.1. Ground Effect

In accordance with the FSAE competition regulations (regulation T.7.6.1), the maximum height that the lowest part of the airfoil of this wing configuration can be positioned in relation to the ground is 107 mm. However, to analyze the behavior of the C_L at different heights, positions in a range of 50 to 375 mm were simulated. The sensitivities of the C_L in response to the variation in the height of the front wing positioning are shown in Figure 9.

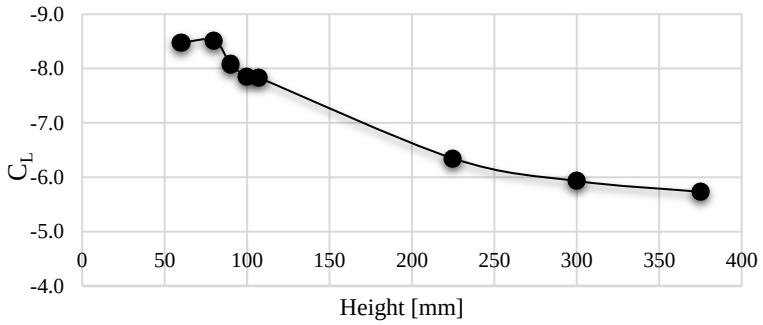

Figure 10. Behavior of the C_L as a function of the height variations of the front wing in relation to the ground.

C_L presented the highest value when the wing was positioned at a height of 80 mm (Figure 10). Thus, the front wing with the end plate 2 profile was placed at this ground clearance in the final assembly of the car for the analysis of the new aerodynamic package.

3.3.2. Foot plates

To verify the influence of foot plates, these were added to the wing with the end plate (2) profile. A curvature in this element was also tested, aiming to deflect some of the flow that would arrive in the front tires.

However, end plate (2) geometry is the profile with foot plates, numbered 2.1 and 2.2 (Table 8). These profiles are only model 2, a flat plate plus rectangular foot plates and model 2.2 a curved plate with a foot plate that accompanies its outline. In this way, the Frame 6 exposes an upper view of the front wing with the two models tested.

Table 8. Variations of the front wing with model 2 of end plates plus foot plates.

N°	Upper view	N°	Upper view
2.1		2.2	

Compared to the simple model 2, the 2.1 (Table 8) model showed a 7.76% increase in C_L versus a 4.54% increase in C_D and a 3.08% increase in aerodynamic efficiency, showing the benefit of its use.

The curvature in the end plate 2.2 and the extension in the profiles to accompany this modification caused an increase in the frontal area of the wing and, consequently, in the C_D. In addition, as can be seen in Table 6, the aerodynamic efficiency was lower in the 2.2 model. However, the support produced by this geometry expresses an increase of 7.55 % in the C_L, a value very close to that of the 2.1 model.

Table 9. Summary of the aspect ratios and aerodynamic characteristics of the model 2 of end plates with the addition of foot plates.

End Plates profile	C_D	C_L	$-C_L/C_D$
2.1	0,7993	-5,3556	6,7007
2.2	0,8318	-5,3455	6,4264

The flow behavior (Table 9) regarding the interaction of the front wing mainly with the components of the suspension subsystem, models 2.1 and 2.2 were mounted on the prototype. The CAD for this simulation has already included the rear wing model chosen in the previous step.

Figure 11 shows the chain lines that represent the flow that passes through the wing and arrives in the front tires for the two models studied.

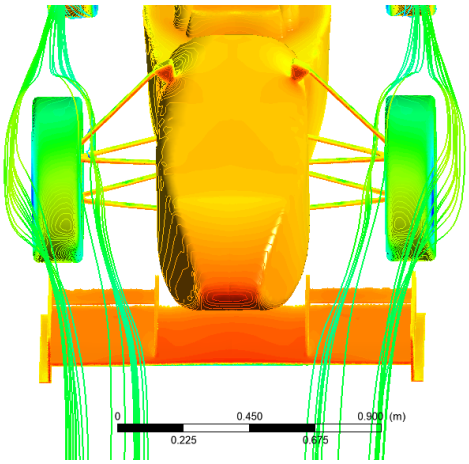

Figure 11.a) Flow behavior when passing through the wing with end plates 2.1 model

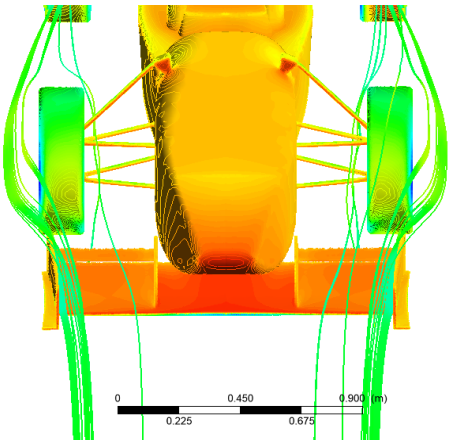

b) Flow behavior when passing through the wing with end plates 2.2 model.

Table 10 shows the frontal area, the C_D and C_L coefficients, and the aerodynamic efficiency obtained by the simulation.

Table 10. Data from the simulation car with the end plate model 3 on the rear wing and with the models 2.1 and 2.2 on the front wing.

Configuration	Frontal area	C_D	$\mathbf{C_L}$	$\mathbf{-C_L/C_D}$
Model 2.1	1,0141 m²	0,9076	-1,2181	1,3421
Model 2.2	1,0079 m²	0,8984	-1,2019	1,3378

Individually, the 2.2 model demonstrated lower performance. However, as can be seen in Table 5, the assemblies with the two models expressed little significant differences in the results. In addition, Figure 13.b shows that the curvature modeled on the end plate 2.2 better conducts the flow out of the front tires, contributing to the reduction of drag, as evidenced by the lower value of the C_D.

Since the characteristics remained similar, the context of the project prioritized the lowest $\mathbf{C_D}$ and, therefore, the 2.2 model will integrate the front wing.

3.4. Analysis of the new aerodynamic package

The rear wing has been placed in the highest position allowed by the regulations, so that the upper end of the end plate is at a height of 1.2 m above the ground. The other positions were maintained. Similarly, only the height of the front wing positioning was modified so that it was placed at the set height of 80 mm above the ground.

Comparation between three configurations are in Table 11 in which brings together the characteristics frontal area, $\mathbf{C_D}$ and $\mathbf{C_L}$ and aerodynamic efficiency. The initial design without aerodynamic package and. The initial design front and rear wings, also and of the final design after the modifications in the end plates and positioning of the wings

Table 11. Comparison between the three sets: initial design without aerodynamic package, initial design with front and rear wings, and final design after wing changes.

Configuration	Front Area	C_D	C_L	$\lvert C_L/C_D \rvert$
Without package aerodynamic	0,8129 m²	0,8247	0,4287	0,5198
Initial package aerodynamic	1,0005 m²	0,9046	-1,0016	1,1072
Final package aerodynamic	1,0079 m²	0,8984	-1,2019	1,3378

The addition of wings considerably increases the projection of the area perpendicular to the flow. Thus, an increase in C_D is also expected. Still, this increase for both models with wings reflects a small penalty that can be offset by the significant gain in the ability to generate down force.

The wing modifications resulted in 0.68% reduction in the C_D, 20.0% increase in the C_L and 20.82% improvement in aerodynamic efficiency. In addition, the change in the flow profile caused using the wings reduced the recirculation of air in the region behind the cockpit. Figure 12 illustrates in a longitudinal plane passing through the center of the car, the flow behavior in the model without aerodynamic package and in the final model.

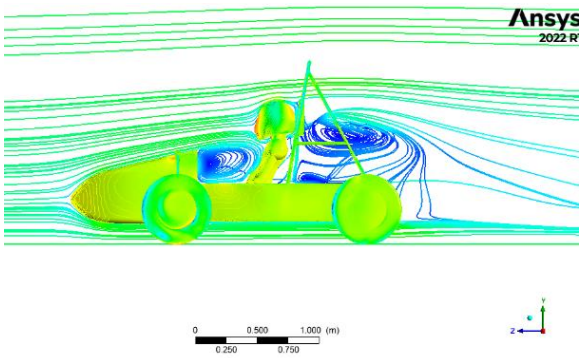

Figure 12. a) Lateral view of the current lines representing the flow profile in the initial wingless model.

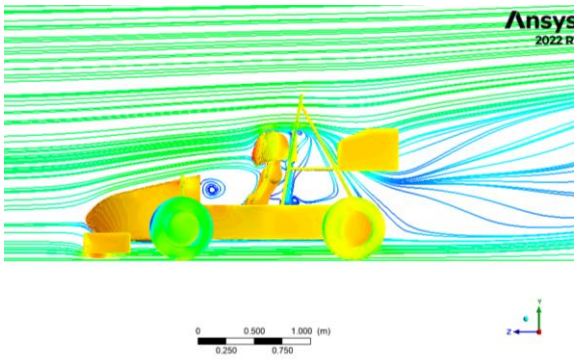

b) Lateral view of the current lines representing the flow profile in the final model

4. CONCLUSIONS

The CFD simulation was possible to predict the aerodynamic coefficients, observe the pressure distributions and the shape of the flow around the vehicle. But even if the computer simulation provides results close to those obtained in real tests, to determine the benefit of the wings it is still necessary to validate through experiments for wind tunnel investigation or on-track tests.

The methodology used was possible to determine the configuration that presented the highest aerodynamic efficiency among the simulated models. As for the effects, the rear wings obtained the following values of C_D, $C_{L,}$ and C_L/C_D of 1.0149, -5.1210, and 5.0458, and for the front wings of 0.7993, -5.3556 and 6.7007, respectively. The aerodynamic efficiency (C_L/C_D) of the assembly installed in the vehicle was - 1.3378, where the coefficients C_D and C_L obtained the values 0.8984 and -1.2019, respectively. In addition, the final C_D of 0.8984 is 25.1 % lower than the maximum acceptable stipulated for the project, of 1.200.

In future projects, with more power available so that aerodynamics can be improved, the increase in the number of wing elements and the automatic activation of the profiles can be studied. In this way, two configurations can be thought of, one focused on reducing drag on acceleration paths and another that prioritizes down force and stability in corners.

5. ACKNOWLEDGEMENTS

We thank Fapemig, Universidade Federal de Viçosa for support this work.

6. REFERENCES

ANSYS, Inc. *ANSYS Fluent User's Guide*. Release 2020 R1. Canonsburg, 2020.

ANSYS, Inc. *ANSYS Meshing User's Guide*. Release 2020 R1. Canonsburg, 2020.

BARBOSA, Lucas Melo Queiroz. *Influência da Aerodinâmica em um Carro de Fórmula SAE***.** Monografia (Trabalho de Conclusão de Curso em Engenharia Mecânica) - Universidade Federal de Uberlândia. Uberlândia, 2018.

LANFRIT, Marco. *Best practice guidelines for handling automotive external aerodynamics with FLUENT*. Version 1.2. Darmstadt, 2005.

MAIA, Rangel Silva. *Desenvolvimento de uma Metodologia para a Análise de Aerofólios com Aplicação no Automobilismo Baseada em Simulações Numéricas***.** Monografia (Trabalho de Conclusão de Curso em Engenharia Automotiva) - Universidade de Brasília. Brasília, 2015.

MCBEATH, Simon. *Competition Car Aerodynamics: A Practical Handbook*. 3ed. Veloce Publishing, 2017.

SAE INTERNATIONAL. *Formula SAE Rules 2022*. V. 2.0, 2021. Disponível em: < file:///C:/Users/ainar/Documents/UFV/2021%20-%20PHT/MEC%20495/FSAE_Rules_2022_V2.pdf>. Acesso em: 05 dez. 2021.

SOLIMAN, Paulo Augusto. *Aerodinâmica em Formula SAE: Processo de Projeto com Foco em Dirigibilidade***.** Monografia (Trabalho de Conclusão de Curso em Engenharia Mecânica) - Universidade Federal de Santa Maria. Santa Maria, 2015.

7. RESPONSIBILITY NOTICE

The authors are the only ones responsible for the printed material included in this paper.